Simple Design for DNA Nanotubes from a Minimal Set of Unmodified Strands: Rapid, Room-Temperature Assembly and Readily Tunable Structure

Graham D. Hamblin, Amani A. Hariri, Karina M. M. Carneiro, Kai L. Lau, Gonzalo Cosa,* and Hanadi F. Sleiman*

Department of Chemistry, McGill University, 801 Sherbrooke Street West, Montreal, QC H3A 0B8 Canada

ABSTRACT DNA nanotubes have great potential as nanoscale scaffolds for the organization of materials and the templation of nanowires and as drug delivery vehicles. Current methods for making DNA nanotubes either rely on a tile-based step-growth polymerization mechanism or use a large number of component strands and long annealing times. Step-growth polymerization gives little control over length, is sensitive to stoichiometry, and is slow to generate long products. Here, we present a design strategy for DNA nanotubes that uses an alternative, more controlled growth mechanism, while using just five unmodified component strands and a long enzymatically produced backbone. These tubes form rapidly at room temperature and have numerous, orthogonal sites available for the programmable incorporation of arrays of cargo along their length. As a proof-of-concept, cyanine dyes were organized into two distinct patterns by inclusion into these DNA nanotubes.

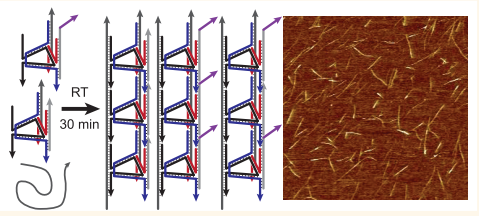

KEYWORDS: DNA nanotechnology · nanotubes · self-assembly · addressable scaffolds

Nanoscale scaffolds that are well-defined and addressable are of particular interest for the production of molecular assembly lines, the templation of nanoelectronic and photonic systems, and the design of targeted drug delivery systems.[1] In constructing such systems, DNA is an especially promising material. Synthetic DNA is commercially available, and its interactions are completely programmable through sequence-specific base pairing. As a biological molecule it is also compatible with enzymatic production methods, increasing the scope of potential applications. As well, short DNA strands possess a relative lack of immunogenicity when compared to peptide-based nanomaterials.[2]

In light of these properties, DNA has been used for the development of a range of self-assembled nanostructures with varied shape, size, and functionality.[3] Originally, these relied primarily on tile-based assembly. Rigid tiles were made up of oriented duplexes with addressable sticky ends and were assembled into discrete structures or repeating arrays.[4] More recently, simplified versions of this strategy have been developed in which the "tiles" are single DNA strands.[5,6] Although a wide range of structures is accessible by tile-based assembly, they all rely on a step-growth polymerization mechanism, where monomers first react to form dimers, then trimers, and eventually long polymers. This is not always an issue for small, discrete objects, but larger DNA tubes and arrays begin to resemble synthetic polymers and can suffer from analogous limitations. Step polymerization is characterized by poor size control and requires nearly quantitative monomer conversion before large polymers are produced. As well, it is highly dependent on correct stoichiometry to avoid stalling growth. For DNA assembly, these factors have made it difficult to control the large-scale dimensions of structures that are grown from small tiles. In addition, they have often necessitated the use of complete sequence symmetry to circumvent stoichiometry issues,[7] which comes at the cost of addressability. Further, growth is extremely sensitive to the DNA structure, curvature, and

* Address correspondence to hanadi.sleiman@mcgill.ca.

Received for review August 13, 2012 and accepted March 1, 2013.

Published online March 01, 2013
10.1021/nn4006329

defects within the tile, often making the use of corrugated designs and careful adjustment of flexibility necessary before large products can grow.[8]

With the development of DNA origami,[9] a new growth mechanism for DNA assembly was introduced. In this case, a single long strand templated the final structure, so that no formal polymerization of units was required to access large objects. Origami gives excellent control over the size and shape and is relatively insensitive to stoichiometry. It has recently been expanded from two-dimensional designs to three-dimensions[10] and can even include complex curvature.[11] However, this level of structural complexity requires the use of hundreds of staple strands, each with a different sequence, as well as long annealing times.

One of the key challenges of DNA design is to find a balance between complexity and ease of synthesis: to make a system that achieves sufficient resolution for the intended application from a minimum number of components. As an organizational scaffold, DNA origami can place many unique targets at a theoretical resolution of about 6 nm,[12] but at the cost of numerous constituent strands. When a lower resolution is acceptable, however, different designs can prove more practical. Here, we present a simple, rapid strategy to build well-defined DNA nanotubes, while retaining minimal complexity and without relying on a step-growth polymerization mechanism. Built from five unmodified component strands and an enzymatically produced backbone, the nanotubes display a repeating attachment site on which DNA-tethered cargo can be hybridized to produce linear arrays. The design relies on a constant core "rung" unit with a single variable binding region, such that replacing one component strand can result in a new nanotube with completely different addressable regions. This trend could be continued to three or more repeating units, allowing practical access to a variety of scaffold configurations. Compared to current tile-based DNA nanotube designs,[13−15] this approach allows rapid, isothermal, templated growth while requiring significantly fewer components than DNA origami nanotubes.[16−18]

RESULTS AND DISCUSSION

We have previously developed DNA nanotubes that are based on a triangular rung, a long continuous backbone produced by rolling circle amplification (RCA), and a set of linking strands.[19] The resulting nanotubes had templated length and consistent, rapid growth properties even at low reactant concentrations. The continuous backbone avoided the step-growth polymerization mechanism and also resulted in increased serum stability over normal DNA. As well, these nanotubes were able to enter HeLa cells with high efficiency compared to duplex DNA, while being compatible with encapsulation and release behavior that we have shown elsewhere.[20] However, this design was based on a synthetically modified, cyclic DNA triangle, requiring access to synthetic chemistry facilities and an in-house DNA synthesizer. In addition, the three-component growth mechanism (backbone, rungs, and linkers) introduced opportunities for tube branching and cross-linking. As such, careful control over stoichiometry and annealing conditions was still required to obtain the desired products.

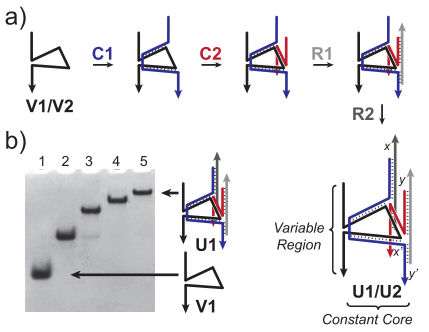

Figure 1. Design of triangular rung unit U1. (a) Variable strand V1 (black) can bind with complementary strand C1 (blue), which spans the internal section and brings the two variable components together, creating a unique variable region for binding. Complementary strand C2 (red) binds the third edge. Rigidifying strands R1 and R2 (gray) bind the overhangs of C1 and C2, holding them out of plane from the triangular core to create the "struts" of the rung. The rigidifiers bind such that three base sticky ends remain at each strut end, which are complementary to each other (denoted *x*, *y*, *x*′, and *y*′). The rigidifying strands R1 and R2 can be terminated with different overhang sequences, allowing the positioning of materials into different patterns (see Figure 4). A new strand, V2, with identical internal sequence with V1 but unique terminal sections, can replace V1 to produce a new unit with new addressability (U2). (b) 8% Native PAGE analysis of the sequential assembly of the unit U1. Lane 1: V1, lane 2: V1+C1, lane 3: V1+C1+C2, lane 4: V1+C1+C2+R1, lane 5: V1+C1+C2+R1+R2.

Here, we designed a new triangular rung unit (**U1**) that uses completely unmodified, linear strands, as outlined in Figure 1. At one corner it has a single-stranded binding region, while at the other two it is self-complementary, *via* very short single-stranded sticky ends (3 bases, labeled *x*, *y*, *x*′, and *y*′). These were designed to be too weak to interact in solution, but strong enough to close when units are held together through their binding regions (see Supporting Information for details). This negates the need for separate linkers, simplifying assembly and minimizing branched or cross-linked products. **U1** was produced by combining equimolar amounts of its component strands and annealing from 95 °C to room temperature over 45 min. Note that a large number of rungs with different variable regions can be generated, merely by modifying one of their constituent strands. Thus, by replacing black strand **V1** for an alternate with identical internal sequence, but a new variable region (**V2**), a new rung can be constructed with different addressability (**U2**).

Upon adding a dimerizing backbone $\mathbf{D_1}$, with two repeats complementary to the variable binding region, unit **U1** is cleanly converted into a stacked dimer

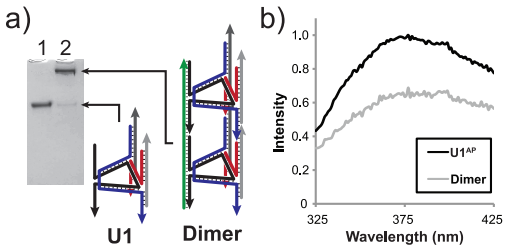

Figure 2. Dimerization of U1. (a) 8% Native PAGE analysis. Lane 1: U1, lane 2: dimer formed upon adding strand D_1, with two repeats of the U1 variable binding region. (b) 2-Aminopurine fluorescence quenching confirms the intended closure of U1 sticky ends upon dimerization. $U1^{AP}$ was created by replacing strands R1 and R2 with $R1^{AP}$ and $R2^{AP}$, and its fluorescence monitored before and after addition of D_1.

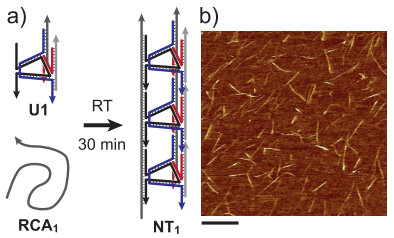

Figure 3. Nanotube formation. (a) RCA_1, a long strand with repeating binding sites for U1 produced by rolling circle amplification, is combined with U1 to produce DNA nanotubes NT_1 in 30 min at room temperature. (b) Atomic force microscopy characterization of NT_1. Phase image, scale bar is 1 μm.

(Figure 2a) in a few minutes at room temperature. To confirm that the sticky ends close as intended, one adenine was replaced with 2-aminopurine in each sticky end. This nucleotide analogue has a decreased quantum yield for fluorescence at 371 nm upon base pairing with thymine. Thus, by monitoring fluorescence before and after the addition of **D_1**, sticky-end closure can be confirmed (Figure 2b). Note that this optimized design was obtained after a number of iterations in which we varied the (i) size of the rung edges, (ii) the junction geometry, and (iii) the sticky-end cohesion length (see Supporting Information).

With this confirmation of correct unit behavior, an RCA backbone strand was next generated with repeating binding regions for **U1**, as previously reported (**RCA_1**).[19] Incubation at room temperature of **U1** and **RCA_1** gave DNA nanotubes composed of repeating **U1**s (**NT_1**), with an average length of 0.64 $\pm$ 0.24 μm, which corresponds well with the RCA product length ($\sim$0.60 μm weighted average), as outlined in Figure 3. Note that the variability in nanotube length is a result of the RCA product distribution. The linear patterning and horizontal dimensions, however, are both structurally well-defined. We have previously shown that a purified RCA fraction can be used to target specific length ranges.[19] In addition, we[21] and others[17] have demonstrated success in producing nearly monodisperse nanotubes. However, as previously discussed, this requires a very large number of unique strands. Instead, this report describes the facile assembly of nanotubes from a small number of starting materials, for applications where the focus is on cargo patterning and where a degree of polydispersity in overall length is acceptable.

This rapid, room-temperature assembly of well-defined nanotubes is most likely facilitated by the templated growth mechanism. Without the need for step-growth polymerization of individual units, fully grown nanotubes can develop quickly and reproducibly. By avoiding separate linkers, a thermal anneal is no longer necessary since branching and cross-linking are less likely. Many of the potential applications for DNA nanotechnology involve sensitive cargo, so a system that does not require harsh thermal anneals for its final assembly is of special interest. Potentially, this could also allow for assembly in cells or other biologically relevant media.

The real strength of this design lies in its conceptual division between a constant core and a variable binding region. By replacing strand **V1** with **V2**, which is identical except for a different binding sequence (Figure 1), a whole new unit (**U2**) can be produced at the cost of just one more strand. The other components (**C1**$-$**2**, **R1**$-$**2**) remain the same; so if a chemically modified (*i.e.*, valuable) strand is required for labeling, it can be used with either unit. Thus, nanotubes with the same geometry but alternating addressability can be generated using **U1**, **U2**, and an RCA backbone with an alternating pattern of complementary sequences to these two units (**$RCA_{1\text{-}2}$**). Indeed, we have confirmed the successful production of such nanotubes (**$NT_{1\text{-}2}$**), with similar properties to **NT_1**. It is important to note that **$NT_{1\text{-}2}$** does not properly form if one of the rungs is not incorporated into the structure, instead yielding highly bundled products under the same conditions (see Supporting Information for details). This trend toward increasingly complex patterning could be continued, with each new component requiring just a single extra variable strand. This is in contrast to tile-based nanotubes, where a whole new tile would be required as well as altered sticky ends in the original one to achieve the same result. DNA origami, on the other hand, requires a different chemically modified strand for every single labeling site, greatly increasing the cost for arrays with many labeling sites.

To illustrate the versatility of this approach, we made a set of component strands with overhang sequences, which can be used for attaching cargo. This was done with rigidifying strands with overhang sequences (**$R1_{ovhgA}$**, **$R1_{ovhgB}$**, **$R2_{ovhgA}$**, **$R2_{ovhgB}$**). Units that incorporated these strands assembled quantitatively (Supporting Information). Together, this set of addressable units could be used to construct nanotubes

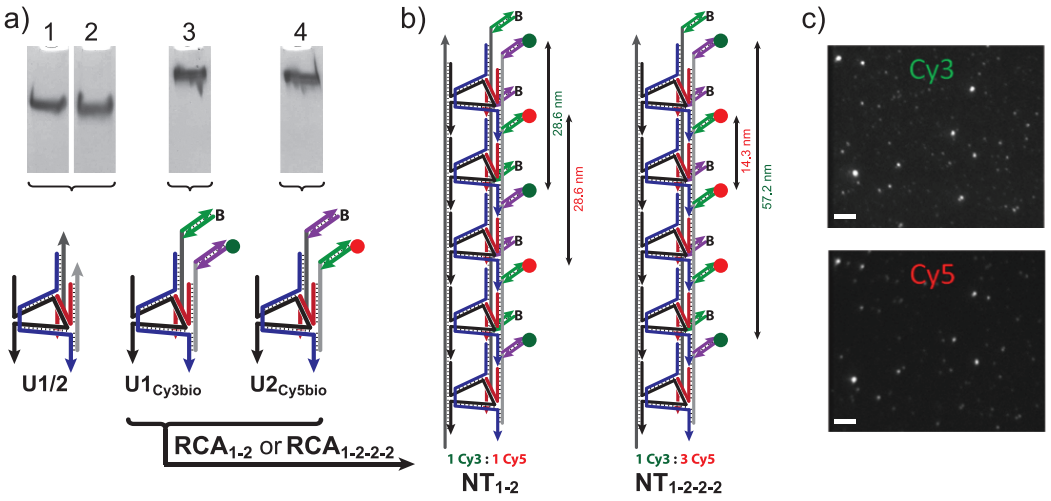

Figure 4. Patterned nanotubes. (a) 8% Native PAGE analysis of various units. Lane 1: U1, lane 2: U2, lane 3: $U1_{Cy3bio}$ (composed of V1, C1, C2, $R1_{ovhgA}$, $R2_{ovhgB}$, Cy3A′, and BiotinB′), lane 4: $U2_{Cy5bio}$ (composed of V2, C1, C2, $R1_{ovhgB}$, $R2_{ovhgA}$, Cy5B′, and BiotinA′). (b) Using RCA_{1-2} for nanotube assembly creates a 1:1 alternating pattern of Cy3 and Cy5 along one side and biotins along another side. Using $RCA_{1-2-2-2}$ for assembly creates a 1:3 pattern of Cy3 and Cy5, also biotinylated. (c) Typical TIRFM images of immobilized nanotubes, showing co-localization of the two fluorophores. Scale bars are 3.3 μm.

with attachment points in various orientations, stoichiometries, and spacing patterns. As an initial proof-of-concept for this capability, we have incorporated the cyanine dyes Cy3 and Cy5 as well as a biotin recognition element as cargo on these nanotubes. Labeled strands with sequences complementary to the overhangs (**Cy3A′**, **Cy5B′**, **BiotinA′**, **BiotinB′**) allowed the selective labeling of either rung unit with any of these cargo molecules. As an example, we created $\mathbf{U1_{Cy3bio}}$, with biotin and Cy3 labels, and $\mathbf{U2_{Cy5bio}}$, with biotin and Cy5 labels (Figure 4a). Upon forming nanotubes with these structures, however, the fluorophore spacing is too small to be resolved by conventional microscopy and too large to produce appreciable Förster resonance energy transfer (FRET). We therefore used single-molecule fluorescence spectroscopy[22−25] conducted on a total internal reflection fluorescence microscopy setup (TIRFM),[26,27] to observe the co-localization of both dyes in the expected stoichiometry for two distinct cargo patterns. The first construct was produced from $\mathbf{U1_{Cy3bio}}$, $\mathbf{U2_{Cy5bio}}$, and the $\mathbf{RCA_{1-2}}$ backbone, yielding a 1:1, alternating pattern of fluorophores along one side and biotins along a second side (Figure 4b).

We exploited single-molecule photobleaching[28−30] as a means to count the number of dyes and thus the overall ratio of green (Cy3) to red (Cy5) emitters in a given nanotube. Polycarbonate film imaging chambers were assembled onto glass coverslips coated with a mixture of polyethylene glycol (PEG) and biotin-tagged PEG to prevent nonspecific adsorption. Individual dye-labeled nanotubes were next specifically immobilized on the chambers *via* biotin−streptavidin interactions (see Supporting Information).[31,32] A low surface density was sought to minimize the possibility of having two nanotubes within a diffraction-limited region. Regions were excited with an evanescent field employing the 638 nm output of a diode laser first and the 532 nm output of a second diode laser next. Photobleaching events were thus recorded sequentially to avoid artifacts in the analysis of photobleaching trajectories arising from bleeding of Cy5 emission into the green channel and of Cy3 emission into the red channel. A total of 60−100 bright fluorescent spots were observed in any given imaged region, with Cy3 and Cy5 emissions co-localizing in space, an indication that the imaged DNA nanotubes contained both Cy3 and Cy5 cargoes (Figure 4c). For each single nanotube imaged, the fluorescence intensity was observed to decrease stepwise over time, giving a "staircase" photobleaching pattern with a measurable number of discrete intensity levels. By manually counting the number of intensity steps recorded for any given nanotube in the red and green channels, the ratio of the "green" and "red" cargo on each nanotube was assessed. More than 100 single nanotubes were analyzed in this way. Figure 5a shows the distribution of the relative number of red and green steps, *i.e.*, green steps/red steps. As expected, a distribution centered around 1:1 Cy3 steps:Cy5 steps ratio was observed for $\mathbf{NT_{1-2}}$.

In generating our second pattern we sought to change the Cy3:Cy5 ratio to a 1:3 value, keeping a maximum of approximately 10 Cy5 dyes per 300 nm long feature. Increasing the density beyond this value would make it harder to differentiate individual bleaching events. As such, we assembled a third RCA backbone ($\mathbf{RCA_{1-2-2-2}}$) that has a single **U1** binding site followed by three **U2** binding sites for each repeat, as shown in Figure 4b. This backbone produced $\mathbf{NT_{1-2-2-2}}$ with a new cargo pattern and stoichiometry. Single-molecule photobleaching analysis demonstrated a

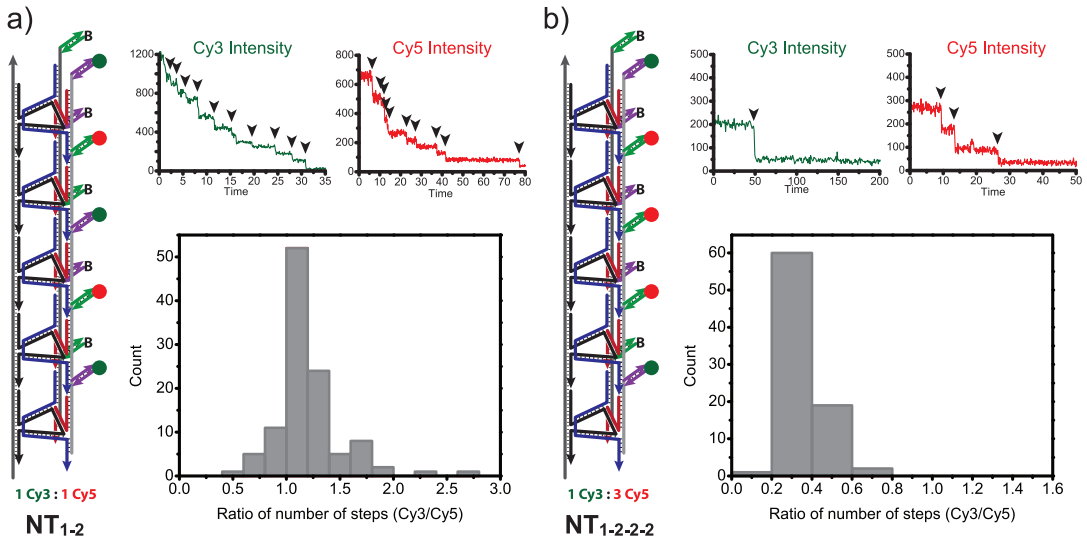

Figure 5. Dye-quantized photobleaching analysis of immobilized nanotubes. (a) NT_{1-2}, with an expected 1:1 Cy3:Cy5 ratio. Typical photobleaching transients for a single nanotube are shown (arrows indicate bleaching events). A histogram displaying the distribution of the ratio of green steps to red steps for individual DNA nanotubes is also shown. The distribution is centered at 1, as expected. (b) $NT_{1-2-2-2}$, with an expected 1:3 Cy3:Cy5 ratio yields a distribution centered at 0.3 as expected.

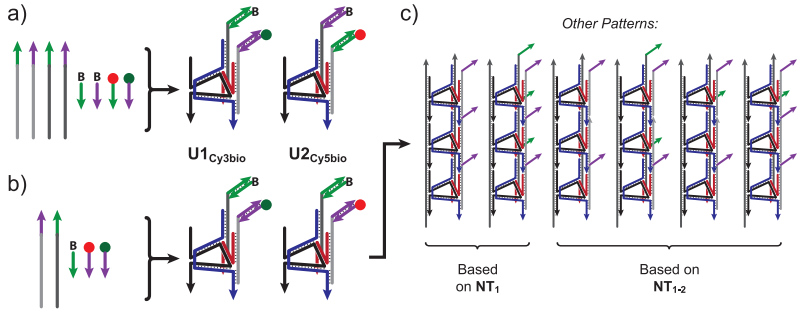

Figure 6. Future patterning. (a) The strategy reported here uses four overhang sequences ($R1_{ovhgA}$, $R1_{ovhgB}$, $R2_{ovhgA}$, and $R2_{ovhgB}$) and four labeled strands (BiotinA′, BiotinB′, Cy3A′, and Cy5B′) to create patterns. (b) A simplified set of strands ($R1_{ovhgA}$, $R2_{ovhgB}$, BiotinB′, Cy3A′, and Cy5A′) could have yielded the same results, but the strands in (a) were already on hand. (c) A wide range of other patterns could be accessed from various combinations of overhang units, cargo, and RCA backbones.

1:3 Cy3:Cy5 ratio on these nanotubes when **$U1_{Cy3bio}$** and **$U2_{Cy5bio}$** were used for assembly (Figure 5b), showing that various cargo patterns are accessible by our design.

Note also that a smaller set of cargo strands could have been used to produce these patterns (the expanded set reported here was used out of convenience, as they were already on hand). Figure 6b outlines how the same result could have been obtained from just **$R1_{ovhgA}$**, **$R2_{ovhgB}$**, **Cy3A′**, **Cy5A′**, and **BiotinB′**. This emphasizes the advantage of having units with unique binding regions but constant cores, such that identical cargo strands can be rendered unique *via* the unit they are attached to. Figure 6c also illustrates examples of additional patterns that are accessible from these strands. Further work toward the organization of other components of interest on these scaffold systems is currently under way.

DNA nanotubes have previously exhibited efficient cellular uptake and encapsulation behavior.[20] Combining these properties with the ability to easily display regiocontrolled heterogeneous patterns of ligands for protection, targeting, and function could yield exciting drug delivery materials. Conversely, scaffolds with precisely positioned components, such as enzymes, gold nanoparticles, polymer chains, or chromophores, are extremely valuable for preparing enzymatic cascades,[33,34] plasmonic tools,[35] and light-harvesting devices,[36] respectively. Being able to generate these rapidly and reproducibly from a minimal set of DNA strands and in a modular fashion will expand these applications and additionally result in assembly in biologically relevant media.

CONCLUSIONS

We have described a rapid, practical design for the construction of DNA nanotubes. They are made from self-complementary core units that will come together only in the presence of an enzymatically produced backbone, *via* addressable binding regions. The final

assembly step is isothermal, avoiding harsh conditions that could be problematic for sensitive cargo, and occurs in just 30 min. The triangular geometry of these nanotubes could be expanded to other shapes, and numerous strand termini are available for labeling overhangs, making them compatible with the complex organization of cargo. As such, they were successfully used to arrange Cy3 and Cy5 fluorophores into two distinct patterns, as confirmed by single-molecule fluorescence spectroscopy analysis. By using a templated growth mechanism, they avoid the limitations of step polymerization while retaining a minimal number of components. We believe that these properties make our design the most balanced, versatile method available for the construction of DNA nanotubes as scaffolds for a wide range of applications.

MATERIALS AND METHODS

Materials. Acetic acid, boric acid, EDTA, urea, magnesium chloride, StainsAll, tris(hydroxymethyl)aminomethane (Tris), D(+) glucose, 2-betamercaptoethanol, and streptavidin were purchased from Aldrich. Nucleoside (1000 Å)-derivatized LCAA-CPG solid support with loading densities of 25−40 μmol/g, Sephadex G-25 (super fine DNA grade), and reagents for automated DNA synthesis were used as purchased from BioAutomation. Exonuclease VII (ExoVII, source: recombinant) was used as purchased from BioLynx Incorporated. Glucose oxidase and catalase were purchased from Roche Applied Science. Acrylamide (40%)/bis-acrylamide 19:1 solution and agarose were purchased from BioShop. Kits for T4 polynucleotide kinase and Quick T4 DNA ligase were purchased from New England Biolabs. A RepliPHI Phi29 reagent set was purchased from Epicentre Biotechnologies for rolling circle amplification. A QIAquick PCR purification kit from Qiagen was used for RCA cleanup. For TIRFM sample preparation, 1% v/v Vectabond/acetone was purchased from Vector Laboratories, while poly(ethylene glycol) succinimidyl valerate MW 5000 (mPEG-SVA) and biotin-PEG-SVA were purchased from Laysan Bio, Inc. Imaging chamber components were purchased from Grace Bio-Lab. Grade SPI-1 highly ordered pyrolytic graphite (HOPG) was purchased from SPI, and AFM cantilevers were from Asylum Research (model AC160TS). TBE buffer (1×) is composed of 90 mM Tris and boric acid and 1.1 mM EDTA, with a pH of ~8.3. TAMg buffer (1×) is composed of 45 mM Tris and 7.6 mM $MgCl_2$, with pH adjusted to 8.0 using glacial acetic acid.

Oligonucleotides. Standard automated oligonucleotide solid-phase synthesis was performed on a BioAutomation MerMade MM6 DNA synthesizer. Optimal strand lengths and geometries were planned with the aid of GIDEON,[37] and sequence design was assisted with the programs CANADA version 2.0 (available online) and NUPACK.[38] Sequences and purification details are given in the Supporting Information. Modified strands were purchased from Integrated DNA Technologies (IDT). Ligation of RCA templates was carried out enzymatically, using T4 Polynucleotide Kinase kit for 5′-phosphorylation and Quick T4 DNA Ligase kit for the ligation. RCA reactions were performed with Phi29 polymerase and purified using a QIAquick PCR purification kit. All oligonucleotides were quantified *via* UV−vis spectroscopy (OD_{260}) using the extinction coefficient ε_{260} as calculated with IDT's OligoAnalyzer.

Preparation of Units U1 and U2. Triangular unit **U1** was generated by the equimolar combination of strands **V1**, **C1**−**2**, and **R1**−**2**, with a final concentration of 436 nM in 1× TAMg. This mixture was annealed from 95 to 20 °C over 45 min to maximize clean product formation. To generate **U2**, the variable strand **V1** was simply replaced with **V2**. Native PAGE (8%, 25 °C, 1× TAMg running buffer, stained with StainsAll) confirmed the clean hybridization of each product, as shown in Figure S1. Optimization of the sticky-end length is discussed in the Supporting Information.

Preparation of Dimer and NT_1. The stacked dimer was produced by addition of 0.5 molar equiv of $\mathbf{D_1}$ to unit **U1** in 1× TAMg, in 30 min at room temperature. Native PAGE (8%, 25 °C, 1× TAMg running buffer, stained with StainsAll) confirmed its clean formation. When strands **R1** and **R2** were replaced with $\mathbf{R1^{AP}}$ and $\mathbf{R2^{AP}}$, 2-aminopurine fluorescence could be followed to confirm sticky-end closure. Fluorescence was monitored with a Fluoromax 2 spectrofluorimeter, using 303 nm excitation wavelength and a 325−425 nm emission window before and after addition of $\mathbf{D_1}$, blanked against addition of 1× TAMg instead. By combining **U1** and $\mathbf{RCA_1}$, nanotube $\mathbf{NT_1}$ could also be prepared in 30 min at room temperature. Nanotubes were characterized by atomic force microscopy (AFM) and Native-PAGE to confirm unit incorporation.

AFM Imaging. AFM was performed on highly ordered pyrolytic graphite with a MultiMode SPM connected to a Nanoscope controller, from the Digital Instruments Veeco Metrology Group. Deposition conditions, supplemental micrographs, and control experiments are given in the Supporting Information.

Preparation of Patterned Nanotubes. Replacing strands **R1** and **R2** with various combinations of overhang strands yielded units with addressable overhang sequences, to which modified strands could be hybridized. $\mathbf{U1_{Cy3bio}}$ was made with **V1**, **C1**, **C2**, $\mathbf{R1_{ovhgA}}$, $\mathbf{R2_{ovhgB}}$, **Cy3A**′, and **BiotinB**′, and $\mathbf{U2_{Cy5bio}}$ was made with **V2**, **C1**, **C2**, $\mathbf{R1_{ovhgB}}$, $\mathbf{R2_{ovhgA}}$, **Cy5B**′, and **BiotinA**′. Assembling these with either $\mathbf{RCA_{1\text{-}2}}$ or $\mathbf{RCA_{1\text{-}2\text{-}2\text{-}2}}$ created nanotubes with biotins along one side and either a 1:1 alternating ratio of Cy3 and Cy5 ($\mathbf{NT_{1\text{-}2}}$), or a 1:3 pattern ($\mathbf{NT_{1\text{-}2\text{-}2\text{-}2}}$). AFM micrographs of $\mathbf{NT_{1\text{-}2}}$ and $\mathbf{NT_{1\text{-}2\text{-}2\text{-}2}}$ are given in the Supporting Information.

Fluorescence Spectroscopy. Coverslips were cleaned, functionalized with polyethylene glycol, and loaded with streptavidin as outlined in the Supporting Information. Nanotubes were immobilized *via* biotin−streptavidin interactions and then imaged with a two-color total internal reflection fluorescence microscopy setup. Photobleaching events were recorded, and the resulting data analyzed with a Matlab routine. More details of sample preparation and imaging conditions are given in the Supporting Information.

Conflict of Interest: The authors declare no competing financial interest.

Supporting Information Available: DNA sequences, detailed experimental procedures, AFM control experiments, TIRFM imaging and analysis. This material is available free of charge *via* the Internet at http://pubs.acs.org.

Acknowledgment. We thank NSERC, the NSERC Vanier Program, CFI, CSACS, CIFAR, and the CIHR Drug Development Training Program for funding. H.F.S. is a Cottrell Scholar of the Research Corporation.

REFERENCES AND NOTES

1. Lin, C.; Liu, Y.; Yan, H. Designer DNA Nanoarchitectures. *Biochemistry* **2009**, *48*, 1663–1674.
2. Guo, P. The Emerging Field of RNA Nanotechnology. *Nat. Nanotechnol.* **2010**, *5*, 833–842.
3. Aldaye, F. A.; Palmer, A. L.; Sleiman, H. F. Assembling Materials with DNA as the Guide. *Science* **2008**, *321*, 1795–1799.
4. Seeman, N. C. An Overview of Structural DNA Nanotechnology. *Mol. Biotechnol.* **2007**, *37*, 246–257.
5. Wei, B.; Dai, M.; Yin, P. Complex Shapes Self-Assembled from Single-Stranded DNA Tiles. *Nature* **2012**, *485*, 623–626.
6. Wilner, O. I.; Orbach, R.; Henning, A.; Teller, C.; Yehezkeli, O.; Mertig, M.; Harries, D.; Willner, I. Self-Assembly of DNA Nanotubes with Controllable Diameters. *Nat. Commun.* **2011**, *2*, 540.

7. He, Y.; Ye, T.; Su, M.; Zhang, C.; Ribbe, A. E.; Jiang, W.; Mao, C. D. Hierarchical Self-Assembly of DNA into Symmetric Supramolecular Polyhedra. *Nature* **2008**, *452*, 198–U141.
8. Yan, H.; Park, S. H.; Finkelstein, G.; Reif, J. H.; LaBean, T. H. DNA-Templated Self-Assembly of Protein Arrays and Highly Conductive Nanowires. *Science* **2003**, *301*, 1882–1884.
9. Rothemund, P. W. Folding DNA to Create Nanoscale Shapes and Patterns. *Nature* **2006**, *440*, 297–302.
10. Douglas, S. M.; Dietz, H.; Liedl, T.; Hogberg, B.; Graf, F.; Shih, W. M. Self Assembly of DNA into Nanoscale Three Dimensional Shapes. *Nature* **2009**, *459*, 414–418.
11. Han, D.; Pal, S.; Nangreave, J.; Deng, Z.; Liu, Y.; Yan, H. DNA Origami with Complex Curvatures in Three-Dimensional Space. *Science* **2011**, *332*, 342–346.
12. Sacca, B.; Niemeyer, C. M. DNA Origami: The Art of Folding DNA. *Angew. Chem., Int. Ed.* **2012**, *51*, 58–66.
13. Rothemund, P. W.; Ekani-Nkodo, A.; Papadakis, N.; Kumar, A.; Fygenson, D. K.; Winfree, E. Design and Characterization of Programmable DNA Nanotubes. *J. Am. Chem. Soc.* **2004**, *126*, 16344–16352.
14. Yin, P.; Hariadi, R. F.; Sahu, S.; Choi, H. M.; Park, S. H.; Labean, T. H.; Reif, J. H. Programming DNA Tube Circumferences. *Science* **2008**, *321*, 824–826.
15. Kuzuya, A.; Wang, R.; Sha, R.; Seeman, N. C. Six-Helix and Eight-Helix DNA Nanotubes Assembled from Half-Tubes. *Nano Lett.* **2007**, *7*, 1757–1763.
16. Ding, B.; Wu, H.; Xu, W.; Zhao, Z.; Liu, Y.; Yu, H.; Yan, H. Interconnecting Gold Islands with DNA Origami Nanotubes. *Nano Lett.* **2010**, *10*, 5065–5069.
17. Douglas, S. M.; Chou, J. J.; Shih, W. M. DNA-Nanotube-Induced Alignment of Membrane Proteins for Nmr Structure Determination. *Proc. Natl. Acad. Sci. U.S.A.* **2007**, *104*, 6644–6648.
18. Fu, Y.; Zeng, D.; Chao, J.; Jin, Y.; Zhang, Z.; Liu, H.; Li, D.; Ma, H.; Huang, Q.; Gothelf, K. V.; *et al.* Single-Step Rapid Assembly of DNA Origami Nanostructures for Addressable Nanoscale Bioreactors. *J. Am. Chem. Soc.* **2013**, *135*, 696–702.
19. Hamblin, G. D.; Carneiro, K. M.; Fakhoury, J. F.; Bujold, K. E.; Sleiman, H. F. Rolling Circle Amplification-Templated DNA Nanotubes Show Increased Stability and Cell Penetration Ability. *J. Am. Chem. Soc.* **2012**, *134*, 2888–2891.
20. Lo, P. K.; Karam, P.; Aldaye, F. A.; McLaughlin, C. K.; Hamblin, G. D.; Cosa, G.; Sleiman, H. F. Loading and Selective Release of Cargo in DNA Nanotubes with Longitudinal Variation. *Nat. Chem.* **2010**, *2*, 319–328.
21. Lo, P. K.; Altvater, F.; Sleiman, H. F. Templated Synthesis of DNA Nanotubes with Controlled, Predetermined Lengths. *J. Am. Chem. Soc.* **2010**, *132*, 10212–10214.
22. Joo, C.; Balci, H.; Ishitsuka, Y.; Buranachai, C.; Ha, T. Advances in Single-Molecule Fluorescence Methods for Molecular Biology. *Annu. Rev. Biochem.* **2008**, *77*, 51–76.
23. Roy, R.; Hohng, S.; Ha, T. A Practical Guide to Single-Molecule Fret. *Nat. Methods* **2008**, *5*, 507–516.
24. Weiss, S. Fluorescence Spectroscopy of Single Biomolecules. *Science* **1999**, *283*, 1676–1683.
25. Moerner, W. E.; Orrit, M. Illuminating Single Molecules in Condensed Matter. *Science* **1999**, *283*, 1670–1676.
26. Marko, R. A.; Liu, H. W.; Ablenas, C. J.; Ehteshami, M.; Gotte, M.; Cosa, G., Binding Kinetics and Affinities of Heterodimeric versus Homodimeric HIV-1 Reverse Transcriptase on DNA-DNA Substrates at the Single-Molecule Level. *J. Phys. Chem. B*, **2013**, in press, DOI: 10.1021/jp308674g.
27. Liu, H. W.; Ngo, A. T.; Cosa, G. Enhancing the Emissive Properties of Poly(p-Phenylenevinylene)-Conjugated Polyelectrolyte-Coated SiO_2 Nanoparticles. *J. Am. Chem. Soc.* **2012**, *134*, 1648–1652.
28. Ulbrich, M. H.; Isacoff, E. Y. Subunit Counting in Membrane-Bound Proteins. *Nat. Methods* **2007**, *4*, 319–321.
29. Casanova, D.; Giaume, D.; Moreau, M.; Martin, J. L.; Gacoin, T.; Boilot, J. P.; Alexandrou, A. Counting the Number of Proteins Coupled to Single Nanoparticles. *J. Am. Chem. Soc.* **2007**, *129*, 12592–12593.
30. Jain, A.; Liu, R. J.; Ramani, B.; Arauz, E.; Ishitsuka, Y.; Ragunathan, K.; Park, J.; Chen, J.; Xiang, Y. K.; Ha, T. Probing Cellular Protein Complexes Using Single-Molecule Pull-Down. *Nature* **2011**, *473*, 484–U322.
31. Ngo, A. T.; Karam, P.; Fuller, E.; Burger, M.; Cosa, G. Liposome Encapsulation of Conjugated Polyelectrolytes: Toward a Liposome Beacon. *J. Am. Chem. Soc.* **2008**, *130*, 457–459.
32. Karam, P.; Ngo, A. T.; Rouiller, I.; Cosa, G. Unraveling Electronic Energy Transfer in Single Conjugated Polyelectrolytes Encapsulated in Lipid Vesicles. *Proc. Natl. Acad. Sci. U.S.A.* **2010**, *107*, 17480–17485.
33. Delebecque, C. J.; Lindner, A. B.; Silver, P. A.; Aldaye, F. A. Organization of Intracellular Reactions with Rationally Designed RNA Assemblies. *Science* **2011**, *333*, 470–474.
34. Wilner, O. I.; Weizmann, Y.; Gill, R.; Lioubashevski, O.; Freeman, R.; Willner, I. Enzyme Cascades Activated on Topologically Programmed DNA Scaffolds. *Nat. Nanotechnol.* **2009**, *4*, 249–254.
35. Tan, S. J.; Campolongo, M. J.; Luo, D.; Cheng, W. Building Plasmonic Nanostructures with DNA. *Nat. Nanotechnol.* **2011**, *6*, 268–276.
36. Dutta, P. K.; Varghese, R.; Nangreave, J.; Lin, S.; Yan, H.; Liu, Y. DNA-Directed Artificial Light-Harvesting Antenna. *J. Am. Chem. Soc.* **2011**, *133*, 11985–11993.
37. Birac, J. J.; Sherman, W. B.; Kopatsch, J.; Constantinou, P. E.; Seeman, N. C. Architecture with Gideon, a Program for Design in Structural DNA Nanotechnology. *J. Mol. Graph. Model.* **2006**, *25*, 470–480.
38. Zadeh, J. N.; Steenberg, C. D.; Bois, J. S.; Wolfe, B. R.; Pierce, M. B.; Khan, A. R.; Dirks, R. M.; Pierce, N. A. Nupack: Analysis and Design of Nucleic Acid Systems. *J. Comput. Chem.* **2011**, *32*, 170–173.